Sensorless Control of Matrix Converter-Fed Synchronous Reluctance Motors Based on Direct Flux Vector Control Method

# Sensorless Control of Matrix Converter-Fed Synchronous Reluctance Motors Based on Direct Flux Vector Control Method

**Arzhang Yousefi-Talouki , Gianmario Pellegrino**
Politecnico di Torino, Turin, Italy
Department of Energy, Corso Duca degli Abruzzi 24, 10129, Torino
Email: arzhang.yousefitalouki@polito.it, gianmario.pellegrino@polito.it

***Abstract:*** *A Sensorless control technique based on direct flux vector control scheme is proposed for matrix converter-fed synchronous reluctance motor drives. The amplitude of stator flux and current component quadrature to stator flux are closed loop controlled in constant switching frequency. A hybrid current-voltage model based flux observer is used so that at low speeds stator flux is estimated through current-to-flux maps and at high speeds, flux estimation is based on back-electromotive force integration. Moreover, a hybrid position and speed observer is proposed in order to estimate rotor position in a wide speed range. At low speeds and also in standstill, rotor position is retrieved based on high-frequency signal injection while at high speeds, back-EMF based model is used to estimate the rotor position. Also, matrix converter is modulated based on indirect space vector modulation. Simulation results for a 2.2 kW synchronous reluctance motor are presented to show the effectiveness of proposed sensorless drive.*

***Key words:*** *Direct flux vector control; High frequency injection; Matrix Converter; Sensorless; Synchronous reluctance motor.*

## 1. Introduction

Matrix converters as ac-to-ac converters have emerged to become an alternative to conventional converters. These converters show attractive advantages such as high quality power output waveforms, bidirectional power flow, and lack of bulky capacitors [1-4].

Synchronous reluctance motors (SyRMs) have been widely adopted in recent years due to their advantages such as low manufacturing cost and simple structures [5-8]. Moreover, due to high saliency features of these machines, SyRMs can be readily adopted to sensorless control methods.

Conventionally, sensorless control methods are categorized into two main control techniques including back-electro motive forced (EMF) based methods and the ones based on high-frequency injection signals. At medium and high speeds, rotor position is estimated based on back-EMF techniques. However, at low speeds and standstill where back-EMF signal is poor, rotor position estimation is inaccurate and impossible at standstill. Therefore, a high-frequency signal, usually voltage, is injected to the motor and high-frequency component of corrsponding current is demodulated and then rotor position is retrieved through a tracking loop.

Direct torque control (DTC) method poses different advantages compared to vector control methods such as fast dynamic and robust implementation. However, variable switching frequency and high torque ripple are the two most drawbacks of this control method [11-12]. Direct flux vector control (DFVC) method which was presented in [13], maintains the main features of DTC and vector control methods such as fixed switching frequency and straightforward limitation of current amplitude. This control operates in stator coordinates $(d_s, q_s)$ where the amplitude of stator flux and current quadrature to stator flux are the two controlled variables. The amplitude of stator flux is regulated using voltage component on $d_s$-axis, while the torque producing current is controlled by means of $q_s$ voltage channel.

Despite the aforementioned advantages of matrix converters and SyR motors, there are a few literature for control of matrix converter-fed synchronous reluctance motor drives [14-15]. Therefore, this paper proposes a sensorless control technique for matrix converter-fed synchronous reluctance motor drives based on direct flux vector control method. To do so, a combined voltage-current model flux observer is adopted. At low speeds, flux observation is based on current model coming from a 2-D current-to-flux tables. While at high speed, flux observation is based on back-EMF integration. In order to cover a wide speed range control, a hybrid speed and position observer is proposed where at low speeds and standstill, high frequency voltage is injected into estimated rotor $\hat{d}$-axis and high frequency component of flux response is demodulated. Provided that in this method high frequency component of flux response is demodulated in place of high frequency component of current response, the cross-saturation effect which may cause to position estimation error is inherently overcome [16]. Above 50 [rpm], high frequency injection starts to be decreased and above 100 [rpm] is completely dropped out and position estimation will be purely base on back-EMF technique.

In the following sections, indirect space vector modulation (ISVM) of matrix converters and its nonlinear errors are briefly investigated and then proposed sensorless technique is studied in details. Eventually, simulation results are presented to

validate the proposed method.

## 2. Matrix converter modulation and nonlinear errors

### *A. Indirect space vector modulation [17]*

The power circuit topology of a three-phase to three-phase matrix converter is shown in Fig.1. Indirect space vector modulation is used to synthetize the output voltage vectors to the input current vectors. The basic idea of this modulation is to separate the matrix converter into a fictitious voltage source rectifier (VSR) and a fictitious voltage source inverter (VSI). Modulation of output voltage vector $(v_o^*, \theta_o^*)$ is done based on VSI while VSR is responsible for control of input phase current $(\theta_{in}^*)$. The phase angles of output voltage and input current vectors are used to determine the output and input sectors, respectively. Fig.2 shows the two adjacent active vector and one zero vector used to synthetize the output and input reference vectors. The duty cycles of four active vectors and one zero vector are expressed as (1) to (5).

$$d_{\mu\gamma} = d_\mu . d_\gamma = \frac{2}{\sqrt{3}} \frac{|V_0^*|}{|V_{in}|} sin\left(\frac{\pi}{3} - \theta_{in}^*\right) sin\left(\frac{\pi}{3} - \theta_0^*\right) \quad (1)$$

$$d_{\mu\delta} = d_\mu . d_\delta = \frac{2}{\sqrt{3}} \frac{|V_0^*|}{|V_{in}|} \sin(\theta_{in}^*) \sin\left(\frac{\pi}{3} - \theta_0^*\right) \quad (2)$$

$$d_{v\delta} = d_v . d_\delta = \frac{2}{\sqrt{3}} \frac{|V_0^*|}{|V_{in}|} \sin(\theta_{in}^*) \sin(\theta_0^*) \quad (3)$$

$$d_{v\gamma} = d_v . d_\gamma = \frac{2}{\sqrt{3}} \frac{|V_0^*|}{|V_{in}|} sin\left(\frac{\pi}{3} - \theta_{in}^*\right) sin(\theta_0^*) \quad (4)$$

$$d_0 = 1 - \left(d_{\mu\gamma} + d_{\mu\delta} + d_{v\delta} + d_{v\gamma}\right) \quad (5)$$

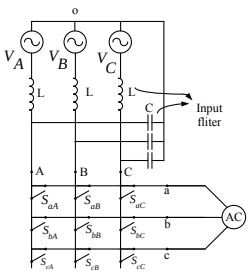


Fig. 1. Schematic diagram of a three-phase matrix converter.

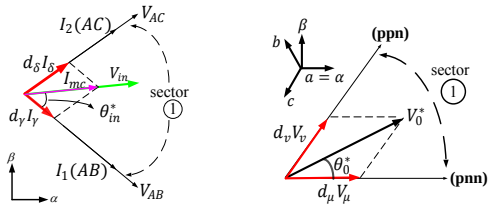


(a) (b)

Fig. 2. Indirect space vector modulation: a) rectification space vector modulation, (b) inversion space vector modulation.

### *B. Matrix converter nonlinear errors [18]*

Similar to conventional converters, matrix converter nonlinear errors come from voltage drop of semiconductors and commutation resulted errors called edge uncertainty effects.

In MCs, two devices are always conducting. The forward voltage of a power device can be approximated by a fixed threshold value $(V_{th})$ which is the average effect of one diode and one IGBT. Thus, the VD is modeled as (6) where $R_d$ accounts for resistance of two devices in series.

$$V_{Di} = 2V_{th} sign\,(I_i) + R_d I_i \;,\; i = \{a, b, c\} \quad (6)$$

When the output voltage is changed from one input phase to the other phase, a voltage is introduced which is dependent to commutation sequence, and commutation pattern. In this paper, a four-step current based commutation is adopted while commutation pattern is double-sided. As an example, it is assumed that the output phase voltage $V_a$ changes from input phase A to input phase B. Fig.3 illustrates the commutation sequence when output phase current $i_a$ is positive and input phase voltage $V_A$ is more positive than $V_B$ where, $t_c$ is commutation time, $t_f$ is IGBT falling time, and $t_{d1}$ and $t_{d2}$ stand for commutation delay. As can be seen, there is a voltage error between ideal voltage $V_a$ and the real one that can be expressed as (7). If Fig.3 is extended to a double-sided switching pattern for one switching period $T_{PWM}$, the ideal and real output phase voltage $V_a$ are as (8) and (9), respectively (for details see [18]), where $T_0$ is the timing of actuating zero vectors and $t_r$ is IGBT rising time. Comparing (8) with (9), it seen that a voltage error is added to the ideal voltage due to the commutation. Generally, the edge uncertainty effect in matrix converters for different input and output sectors is shown as (10) where *j* denotes for input phases and *i* stands for output phases.

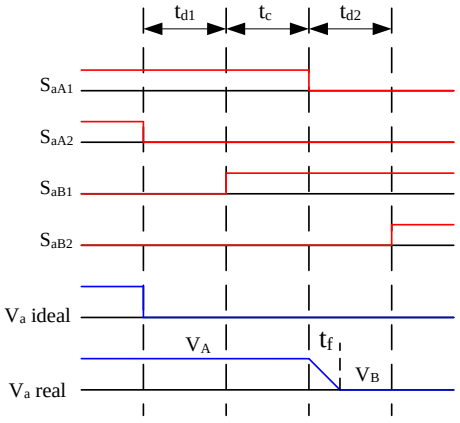


Fig. 3. Four-step current based commutation when output current is positive and input phase voltage $V_A$ is more positive than $V_B$: commutation is from input phase A to input phase B.

$$EU_{A\to B} = V_{AB}(t_{d1} + t_c + t_f) \quad (7)$$

$$V_a = \frac{V_A(T_{PWM}-T_0)}{2T_{PWM}} \quad (8)$$

$$V_a = \frac{V_A(T_{PWM}-T_0)}{2T_{PWM}} + \frac{3V_A(t_c+t_f-t_r)}{T_{PWM}} \quad (9)$$

$$EU_i = \frac{3V_j(t_c+t_f-t_r)}{T_{PWM}} \cdot sign(i_i),\ j = A,B,C,\ \ i = a,b,c. \quad (10)$$

## 3. Direct flux vector control method

In this section DFVC method is investigated briefly. First, SyR motor model in rotor $dq$ frame is analyzed and then model is transferred to stator reference frame $d_s q_s$ since DFVC method operates in stator coordinates. Fig.4 shows the different reference frames adopted in this paper.

### *A. Motor model in rotor frame*

The voltage and torque equations of a SyR motor in rotor frame can be expressed as (11)-(13), where $R_s$ is stator resistance, $p$ is pole pairs numbers, $\bar{\lambda}_{dq}$is stator flux linkage vector, and $L_d$ and $L_q$ are inductances in *d*- and *q*- axis. Equation (13) is implemented in the form of 2-D look up table to include the saturation and cross-saturation effects. Fig.5 illustrates the flux linkage maps for the SyR motor under test, evaluated experimentally.

$$\bar{v}_{dq} = R_s \cdot \bar{\imath}_{dq} + \frac{d\bar{\lambda}_{dq}}{dt} + j\omega \cdot \bar{\lambda}_{dq} \quad (11)$$

$$T = \frac{3}{2}\, p \cdot (\lambda_d i_q - \lambda_q i_d) \quad (12)$$

$$\begin{cases} \lambda_d = \lambda_d(i_d, i_q) = L_d(i_d, i_q) \cdot i_d \\ \lambda_q = \lambda_q(i_d, i_q) = L_q(i_d, i_q) \cdot i_q \end{cases} \quad (13)$$

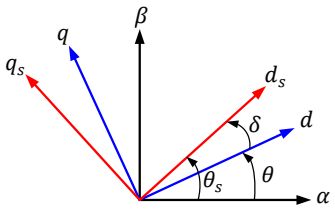


Fig. 4. Reference frames: stator $(\alpha, \beta)$, rotor $(d, q)$ and stator flux$(d_s, q_s)$ coordinates.

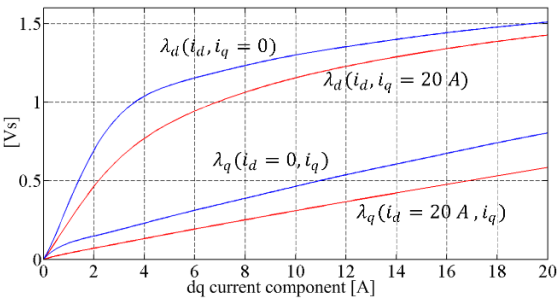


Fig. 5. Flux linkage maps of the SyRM under test, evaluated experimentally.

### *B. Motor model in stator frame*

If voltage and torque equations (11) and (12) are transferred to stator flux coordinates $(d_s, q_s)$, (14) and (15) are obtained where λ is stator flux amplitude. Torque equation (15) can be written also in terms of flux amplitude and phase angle as (16) considering $\lambda_d = \lambda \cdot cos(\delta)$ and $\lambda_q = \lambda \cdot sin(\delta)$.

$$\begin{cases} v_{ds} = R_s i_{ds} + \frac{d\lambda}{dt} \\ v_{qs} = R_s i_{qs} + \lambda(\omega + \frac{d\delta}{dt}) \end{cases} \quad (14)$$

$$T = \frac{3}{2} \cdot p \cdot \lambda \cdot i_{qs} \quad (15)$$

$$T = \frac{3}{2} \cdot p \cdot \frac{L_d - L_q}{2L_d L_q} \cdot \lambda^2 \cdot sin(2\delta) \quad (16)$$

### *C. Direct flux vector control*

The block diagram of sensorless speed-controlled direct flux vector control is depicted in Fig.6. As said, the amplitude of stator flux and current component on $q_s$-axis are the two controlled variables. It is seen from (14) that stator flux amplitude is regulated by means of $v_{ds}$, and load angle is controlled using $v_{qs}$. From (16) it is concluded that by controlling load angle in a given flux amplitude, electromagnetic torque is regulated. However, electromagnetic torque can be controlled using (15) by regulating $i_{qs}$ which is more straightforward compared to (16) and is not dependent to motor parameters. Hence, $i_{qs}$is closed loop controlled for the sake of torque control.

### *D. Stator flux observer*

A combined voltage-current model stator flux observer is adopted in this paper as illustrated in Fig.7. The transfer function of flux observer is as (17) where gain $g[rad/s]$ is a cross over speed between low and high speeds. As can be seen from (17), when the speed is low, flux observation is based on current-to flux maps and while in the opposite, when speed increases, flux observation switches to back-EMF integration. The output of the observer is flux angle $\hat{\theta}_s$ and the amplitude of the flux λ. Stator flux angle is calculated as (18).

$$\hat{\lambda}_{\alpha\beta} = \frac{s}{s+g}\left(\frac{v_{\alpha\beta} - Ri_{\alpha\beta}}{s}\right) + \frac{g}{s+g}(\hat{\lambda}_{\alpha\beta,i}) \quad (17)$$

$$\begin{cases} sin(\hat{\theta}_s) = \frac{\hat{\lambda}_\beta}{|\hat{\lambda}|} = \frac{\hat{\lambda}_\beta}{\sqrt{(\hat{\lambda}_\alpha^2 + \hat{\lambda}_\beta^2)}} \\ cos(\hat{\theta}_s) = \frac{\hat{\lambda}_\alpha}{|\hat{\lambda}|} = \frac{\hat{\lambda}_\alpha}{\sqrt{(\hat{\lambda}_\alpha^2 + \hat{\lambda}_\beta^2)}} \end{cases} \quad (18)$$

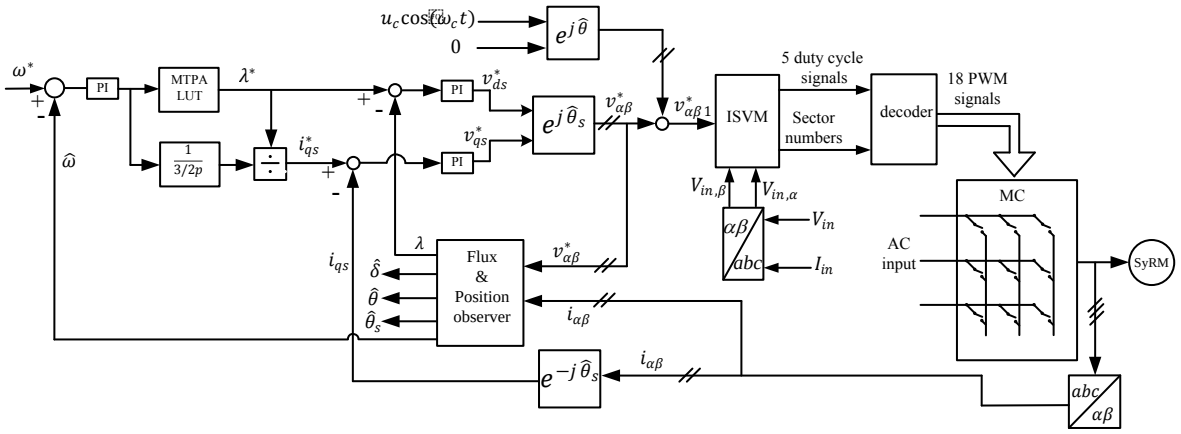


Fig. 6. Sensorless DFVC of matrix converter-fed SyR motor.

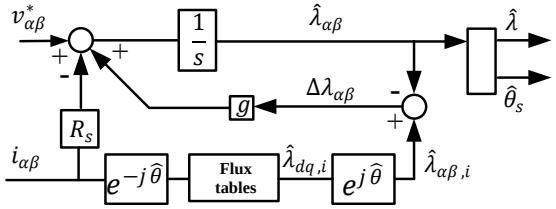


Fig. 7. Stator flux observer.

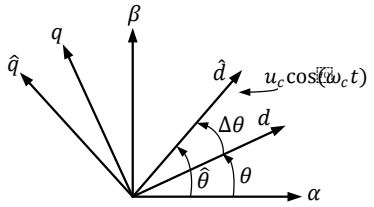


Fig. 8. Actual and estimated rotor reference frame.

## 4. Proposed sensorless control strategy

In order to cover a wide speed range control, a hybrid position observer is proposed in this paper which will be explained in details. Back-EMF based position estimation is assisted with high-frequency signal injection at low speeds, while at high speeds, high-frequency injection is dropped out and rotor position estimation is purely based on back-EMF.

### *A. High-frequency signal injection*

In this paper a high-frequency voltage component (50 [V], 833 [Hz]) is injected to the estimated rotor $\hat{d}$-axis as illustrated in Fig.8. Therefore, the corresponding high-frequency current component in estimated $(\hat{d},\hat{q})$ axis are as (19) and (20). As can be seen from (19), if it is desired that rotor position is retrieved form $I_{\hat{q}h}$, the cross-saturation term, i.e., $L_{dq}\sin(2\Delta\theta)$ should be compensated. Otherwise, an error will be appeared in rotor position estimation. However, from (13) and using current-to-flux maps, (21) is concluded where subscript $i$ means that high-frequency component of flux is coming from current model (flux maps). In the second term of 21, term $[1-cos(2\Delta\theta)]$ can be neglected if it is assumed that $\Delta\theta$ is a small angle. Therefore, (22) will be concluded.

$$\begin{cases} I_{\hat{d}h} = k\cdot[L_{cm} - L_{dm}\cos(2\Delta\theta) - L_{dq}\sin(2\Delta\theta)] \\ I_{\hat{q}h} = k\cdot\left[L_{dm}\sin(2\Delta\theta) - L_{dq}\cos(2\Delta\theta)\right] \end{cases} \quad (19)$$

$$\begin{cases} k = \frac{u_c\sin(\omega_c t)}{\omega_c(L_{dd}L_{qq}-L_{dq}^2)} \\ L_{cm} = \frac{L_{dd}+L_{qq}}{2},\ L_{dm} = \frac{L_{dd}-L_{qq}}{2} \end{cases} \quad (20)$$

$$\begin{cases} \lambda_{\hat{d}h,i} = k\left[L_{dd}L_{cm} - (L_{dd}L_{dm})\cos(2\Delta\theta) - L_{dq}L_{cm}\sin(2\Delta\theta)\right] \\ \lambda_{\hat{q}h,i} = k[L_{dq}L_{cm}[1-\cos(2\Delta\theta)] + \left[L_{qq}L_{dm} - L_{dq}^2\right]\sin(2\Delta\theta)] \end{cases} \quad (21)$$

$$\lambda_{\hat{q}h,i} = k\cdot[L_{qq}L_{dm} - L_{dq}^2]\cdot sin(2\Delta\theta) \quad (22)$$

With comparing (22) with (19), it is seen that if high-frequency flux component in estimated $\hat{q}$-axis is demodulated in place of current component, the cross-saturation error will be inherently overcome. If (22) is multiplied by $sin(\omega_c t)$ and then low pass filtered (LPF), an error will be obtained (23) which will be source of a PI regulator to force it to zero. Fig.9 illustrates the tracking loop PLL used in this paper to obtain the rotor position, where $\omega_{HF}$ denotes for observed speed coming from high-frequency injection method.

$$\epsilon = \frac{u_c}{2\omega_c(L_{dd}L_{qq}-L_{dq}^2)}[L_{qq}L_{dm} - L_{dq}^2]sin(2\Delta\theta) \quad (23)$$

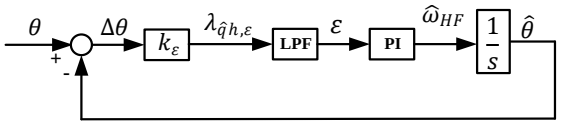


Fig. 9. High-frequency injection-based tracking loop.

### *B. Hybrid Rotor position estimation*

Above a certain speed, rotor position can be obtained using back-EMF information. In this case, rotor position and speed can be obtained using (24), and (25), respectively, where $F_S$ is the sampling frequency and subscript $F$ denotes for position and speed obtained from flux observer.

$$\begin{cases} \sin(\hat{\theta}_F) = \frac{\hat{\lambda}_d \cdot \hat{\lambda}_{\beta,i} - \hat{\lambda}_q \cdot \hat{\lambda}_{\alpha,i}}{|\hat{\lambda}_i||\hat{\lambda}|} \\ \cos(\hat{\theta}_F) = \frac{\hat{\lambda}_d \cdot \hat{\lambda}_{\alpha,i} + \hat{\lambda}_q \cdot \hat{\lambda}_{\beta,i}}{|\hat{\lambda}_i||\hat{\lambda}|} \end{cases} \quad (24)$$

$$\hat{\omega}_{F,k} = (\sin\hat{\theta}_{F,k}\cos\hat{\theta}_{F,k-1} - \cos\hat{\theta}_{F,k}\sin\hat{\theta}_{F,k-1}).F_S \quad (25)$$

As said, rotor position estimation based on back-EMF is assisted with high-frequency injection method. Fig.10 shows the proposed position observer. As can be seen, a gain $k$ is inserted in the high-frequency injection loop. Below 50 [rpm], $k$ equals to 1 and above 100 [rpm], $k$ becomes zero which means that high-frequency injection is dropped out completely.

It should be noted that since there is no magnet in pure SyR motors, a minimum flux always is needed to ensure minimum excitation to the motor. This lower limit of flux amplitude is considered 0.7 [Vs] in this paper.

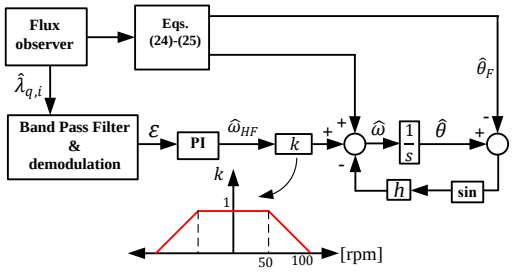


Fig. 10. Proposed combined rotor position observer.

## 5. Simulation results

In this section simulation results are presented to validate the proposed method. The synchronous reluctance motor and MC data is tabulated in Table 1. A simple method is adopted for MC nonlinear error compensation [19]. The results are presented in different speed and load levels.

Table 1 - SyR Machine under test specifications

| **SyR motor** | |
|---|---|
| Rated power/Number of poles | 2.2 kW / 4 |
| Nominal Speed/Rated Torque | 1500 rpm / 14 Nm |
| Phase resistance | 3.5 Ω |
| Moment of inertia ($J$) | 0.005 $kg.m^2$ |
| EUPEC FM35R12KE3ENG module | |
| Power devices | 1200 V, 35 A, IGBT |
| $t_c$ | 0.3 $\mu s$ |
| $t_f$ / $t_r$ | 65-90 ns / 30-45 ns |

Fig. 11 shows the drive performance at standstill. Estimated and actual speed, electromagnetic torque, current on $q_s$-axis, flux amplitude, rotor position error, and three-phase currents are shown in this figure. 14 [Nm] step load is applied at $t = 3\ s$ and again removed at $t = 7\ s$ when the motor speed reference is zero. As can be seen, rotor position estimation error is around zero and dynamics of the system is fairly good.

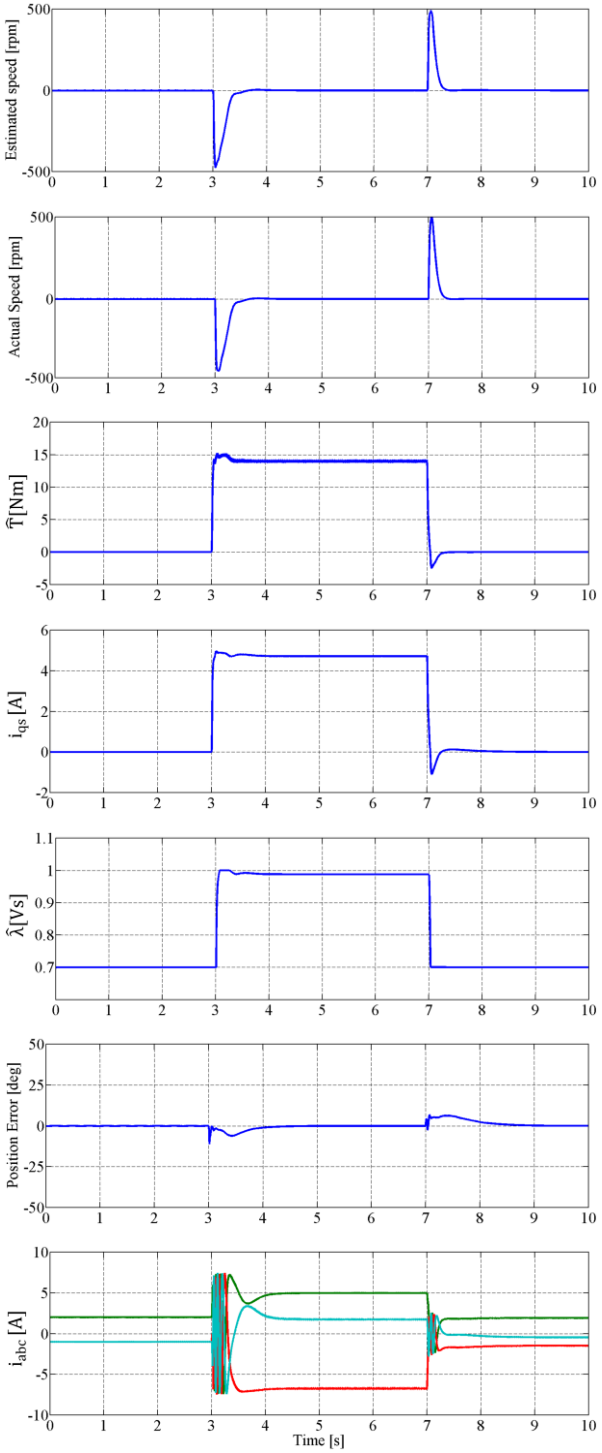


Fig. 11. Performance of the drive at standstill with full-load step load torque.

Fig.12 shows the performance of the proposed sensorless controller at low speeds. At $t = 5\ s$ the speed is reversed from 50 [rpm] to -50 [rpm] under full-load condition. The estimated and actual speeds, electromagnetic torque, $i_{qs}$, stator flux amplitude, position estimation error, and three-phase currents are depicted in this figure. As it is seen, the position estimation error is very close to zero.

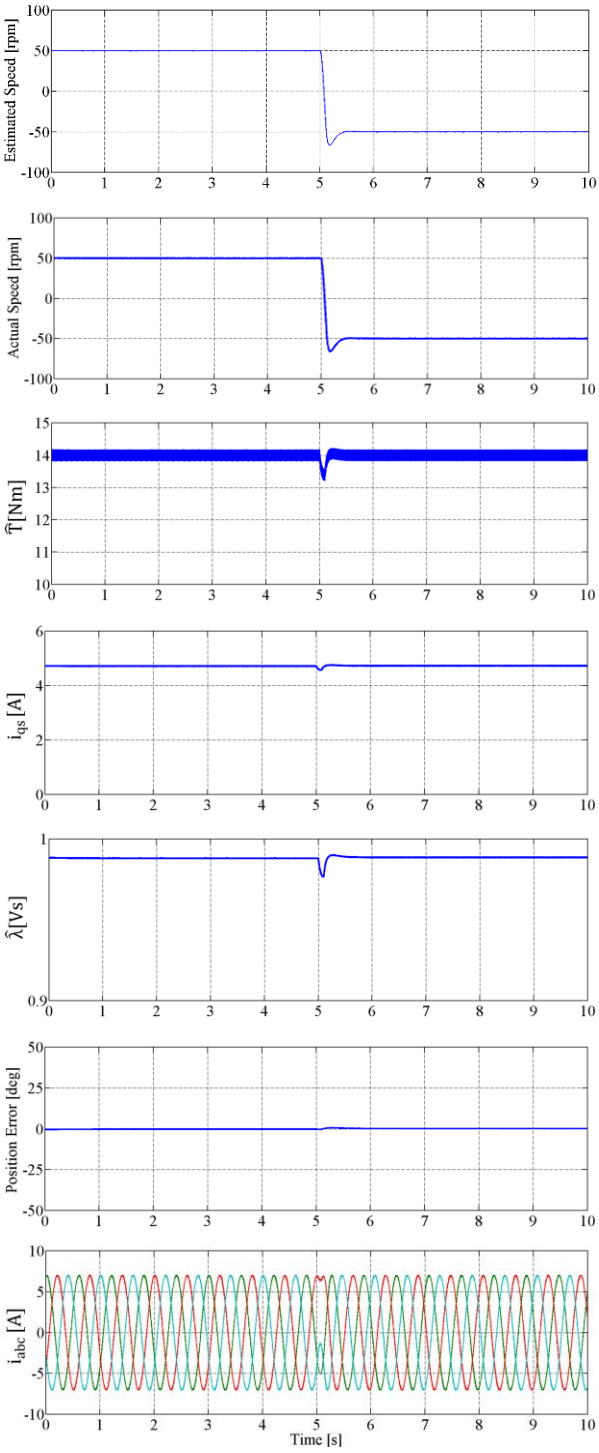


Fig. 12. Full-load speed reversal from 50 [rpm] to -50 [rpm].

Also, the performance of the system at high speeds is investigated in Fig.13. At $t = 1\ s$, 1000 [rpm] step speed command is applied to the drive and at $t = 4\ s$, full load torque is applied to the motor. Similar to low speed conditions, the position estimation error and dynamics of the system are acceptable.

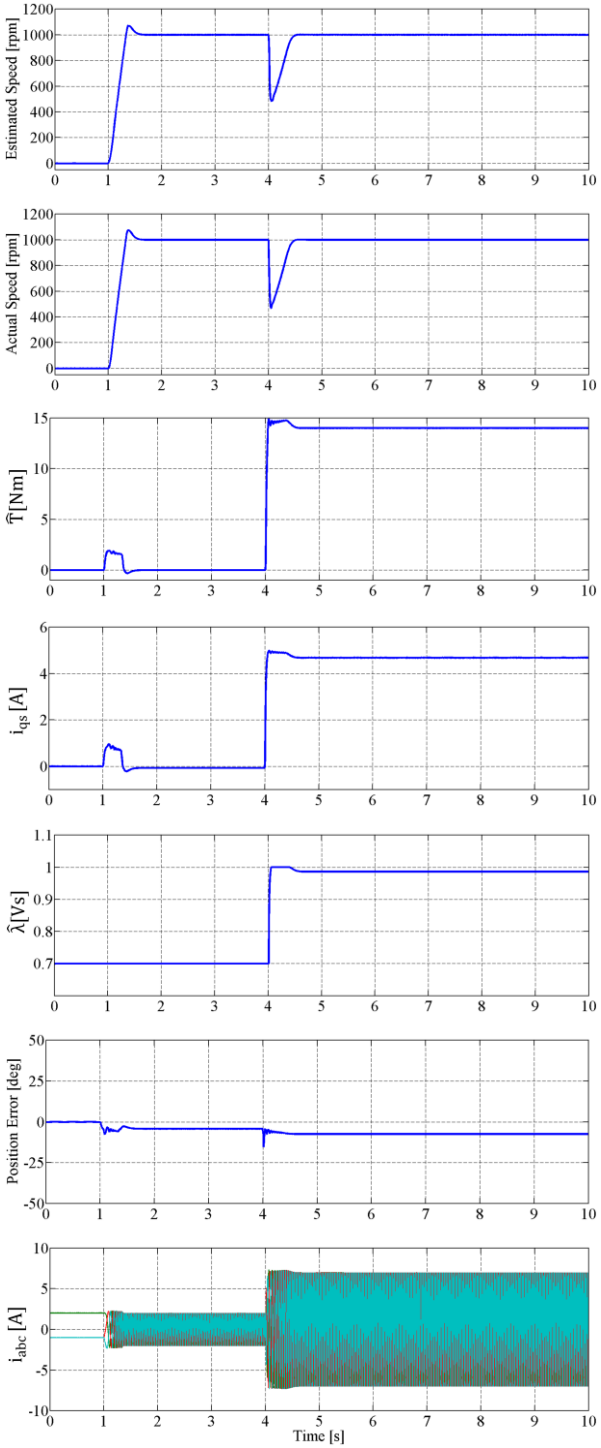


Fig. 13. Performance of the drive at 1000 [rpm] with full-load.

As said, when the speed is above 50 [rpm], high-

frequency injection starts to be deacreased and above 100 [rpm] is dropped out completely. This is sown in Fig.14, where the estimated speed and voltage on $\alpha$-axis has been magnified. It is evident in this figure that, between 50 and 100 [rpm], high-frequency injection is decreasing and above 100 [rpm] is dropped out. Moreover, the performance of the drive is shown in this figure when the speed goes to 1500 [rpm] and again is reversed to -1500 [rpm].

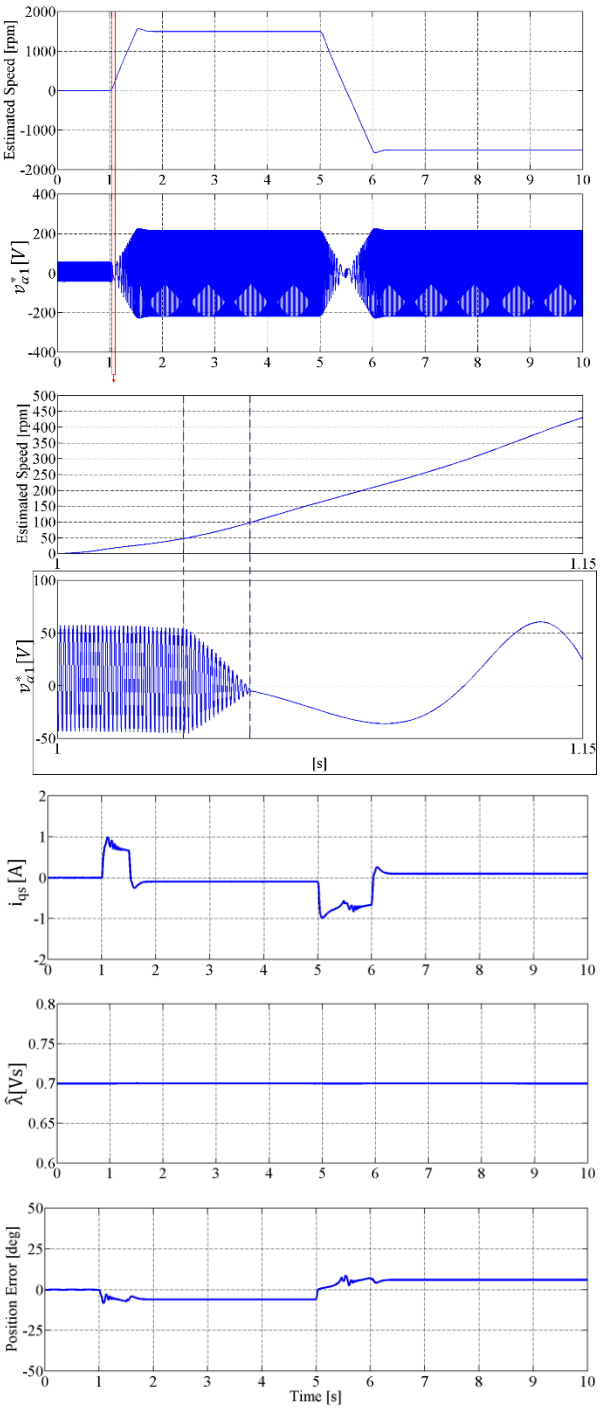


Fig. 14. No-load high speed reversal.

## 6. Conclusion

A sensorless control technique for matrix converter-fed synchronous reluctance motor has been presented in this paper based on direct flux vector control method. A hybrid position observer has been presented to cover a wide speed range control. Below 50 [rpm], rotor position is estimated based on back-EMF method assisted with high-frequency signal injection methods, while above 100 [rpm], high-frequency injection is dropped out and back-EMF method remains alone. The simulation results have been presented for various speed and load levels showing good performance in transients and steady states.

## References


[1] Wheeler, P.W.; Rodriguez, J.; Clare, J.C.; Empringham, L.; Weinstein, A., "Matrix converters: a technology review," Industrial Electronics, IEEE Transactions on , vol.49, no.2, pp.276,288, Apr 2002.

[2] Casadei, D.; Serra, G.; Tani, A., "The use of matrix converters in direct torque control of induction machines," Industrial Electronics, IEEE Transactions on , vol.48, no.6, pp.1057,1064, Dec 2001.

[3] Rodriguez, J.; Rivera, M.; Kolar, J.W.; Wheeler, P.W., "A Review of Control and Modulation Methods for Matrix Converters," Industrial Electronics, IEEE Transactions on , vol.59, no.1, pp.58,70, Jan. 2012.

[4] Yousefi-Talouki, A.; Pouresmaeil, E.; Jørgensen, B.N., "Active and reactive power ripple minimization in direct power control of matrix converter-fed DFIG," International Journal of Electrical Power & Energy Systems, Vol.63, pp. 600,608, Dec. 2014.

[5] Vagati, A.; Pastorelli, M.; Franceschini, G., "High-performance control of synchronous reluctance motors," Industry Applications, IEEE Transactions on , vol.33, no.4, pp.983,991, Jul/Aug 1997.

[6] Boglietti, A.; Cavagnino, A.; Pastorelli, M.; Vagati, A., "Experimental comparison of induction and synchronous reluctance motors performance," Industry Applications Conference, 2005. Fourtieth IAS Annual Meeting. Conference Record of the 2005 , vol.1, no., pp.474,479 Vol. 1, 2-6 Oct. 2005.

[7] Bon-Ho Bae; Seung-Ki Sul, "A novel dynamic overmodulation strategy for fast torque control of high-saliency-ratio AC motor," in Industry Applications, IEEE Transactions on , vol.41, no.4, pp.1013-1019, July-Aug. 2005.

[8] S. Taghavi; P. Pillay, "New Title: A Novel Grain Oriented Lamination Rotor Core Assembly for a Synchronous Reluctance Traction Motor with a Reduced Torque Ripple Algorithm," in IEEE Transactions on Industry Applications , vol.PP, no.99, pp.1-1.

[9] G. H. B. Foo and M. F. Rahman, "Direct Torque Control of an IPM-Synchronous Motor Drive at Very Low Speed Using a Sliding-Mode Stator Flux Observer," in IEEE Transactions on Power Electronics, vol. 25, no. 4, pp. 933-942, April 2010.

[10] Foo, G.; Sayeef, S.; Rahman, M.F., "Low-Speed and Standstill Operation of a Sensorless Direct Torque and Flux Controlled IPM Synchronous Motor Drive," in Energy Conversion, IEEE Transactions on , vol.25, no.1, pp.25-33, March 2010.

[11] Y. Inoue, S. Morimoto and M. Sanada, "Comparative Study of PMSM Drive Systems Based on Current Control and Direct Torque Control in Flux-Weakening Control Region," in IEEE Transactions on Industry Applications, vol. 48, no. 6, pp. 2382-2389, Nov.-Dec. 2012.

[12] Xinan Zhang; Foo, G.H.B.; Vilathgamuwa, D.M.; Maskell, D.L., "An Improved Robust Field-Weakeaning Algorithm for Direct-Torque-Controlled Synchronous-Reluctance-Motor Drives," in Industrial Electronics, IEEE Transactions on , vol.62, no.5, pp.3255-3264, May 2015.

[13] Pellegrino, G.; Bojoi, R.I.; Guglielmi, P., "Unified Direct-Flux Vector Control for AC Motor Drives," in Industry Applications, IEEE Transactions on , vol.47, no.5, pp.2093-2102, Sept.-Oct. 2011.

[14] A. Yousefi-Talouki and G. Pellegrino, "Sensorless vector controlled synchronous reluctance motor fed by matrix converter," *2015 Intl Aegean Conference on Electrical Machines & Power Electronics (ACEMP), 2015 Intl Conference on Optimization of Electrical & Electronic Equipment (OPTIM) & 2015 Intl Symposium on Advanced Electromechanical Motion Systems (ELECTROMOTION)*, Side, 2015, pp. 593-598.

[15] A. Yousefi-talouki and G. Pellegrino, "Vector control of matrix converter-fed synchronous reluctance motor based on flux observer," Electrical Machines Design, Control and Diagnosis (WEMDCD), 2015 IEEE Workshop on, Torino, 2015, pp. 210-215.

[16] Guglielmi, P.; Pastorelli, M.; Vagati, A., "Impact of cross-saturation in sensorless control of transverse-laminated synchronous reluctance motors," in Industrial Electronics, IEEE Transactions on , vol.53, no.2, pp.429-439, April 2006.

[17] Huber, L.; Borojevic, D., "Space vector modulated three-phase to three-phase matrix converter with input power factor correction," Industry Applications, IEEE Transactions on , vol.31, no.6, pp.1234,1246, Nov/Dec 1995.

[18] Arias, A.; Empringham, L.; Asher, G.M.; Wheeler, P.W.; Bland, M.; Apap, M.; Sumner, M.; Clare, J.C., "Elimination of Waveform Distortions in Matrix Converters Using a New Dual Compensation Method," Industrial Electronics, IEEE Transactions on , vol.54, no.4, pp.2079,2087, Aug. 2007.

[19] A. Yousefi-Talouki, G. Pellegrino, M. Mengoni and L. Zarri, "Self-commissioning algorithm for matrix converter, nonlinearity compensation," *2015 IEEE Energy Conversion Congress and Exposition (ECCE)*, Montreal, QC, 2015, pp. 4077-4083.